A fast multipole boundary element method implemented for wet single particle and wall interactions

Adams, Michael; Andrews, James

DOI:
https://doi.org/10.1016/j.powtec.2018.03.029

Document Version
Peer reviewed version

Citation for published version (Harvard):
Adams, M & Andrews, J 2018, 'A fast multipole boundary element method implemented for wet single particle and wall interactions', *Powder Technology*. https://doi.org/10.1016/j.powtec.2018.03.029

A fast multipole boundary element method implemented for wet single particle and wall interactions

James W. Andrews & Michael J Adams

School of Chemical Engineering, University of Birmingham, Edgbaston, Birmingham, B15 2TT, UK
andrewjw@bham.ac.uk

ABSTRACT

The progress is described in developing a parallel computer code to study the dynamics of wet granular systems based on the Fast Multi-pole Boundary Element Method (FMBEM). Here, three examples are considered that have closed-form or numerical solutions and thus able to act as benchmarks. They involved capillary interactions, the formation of a solid-solid contact when a particle approaches a solid wall while immersed in a Newtonian fluid, and the isoviscous hydrodynamic and elastohyrodynamic sliding of a particle. While computationally more expensive than DEM, there are a number of advantages such as extending interactions from the pendular to more saturated states, the ease with which non-spherical particles can be modelled and the ability to model wet granular systems that may exhibit transitions from frictional to lubricated flow. Consequently, FMBEM is able to model wet agglomerates more realistically than DEM and this is important for improving the performance of twin screw granulation, which is the intended application of the current work.

KEYWORDS

Wet granular media, Fast Multi-pole Boundary Element Method, Capillary, Lubrication

1. Introduction

Tablets are the most common oral dosage form for pharmaceutical drugs, which contain primarily the Active Pharmaceutical Ingredients (APIs), fillers, disintegrants and binders. Generally the feed powders are granulated to improve their flow characteristics and thus ensure homogenisation and accurate metering to the tableting dies. High shear wet granulation (HSG) is the most common batch process in which a solution or melt binder is mixed with the feed powders. However, there is a growing interest in continuous granulation processes to improve efficiency and product quality. In

particular, twin screw granulation (TSG) has considerable potential compared to HSG because of its flexibility in terms of the throughput and equipment design, reproducibility, short residence times, smaller liquid/solid ratios and also the ability to granulate difficult-to-process formulations [1]. It involves a self-wiping co-rotating intermeshing twin screw extruder with an open channel at the exit; the screws comprise helical conveying elements (CEs) and mixing segments that are usually kneading elements (KEs). The specification of the granular product includes a tolerance on the size distribution and mechanical strength, which control the dissolution and mechanical strength of tablets formed from the granules. Unlike batch granulation, further work is required to understand the mechanisms and process factors that govern size enlargement at a level of detail required by the FDA regulations (eg Quality by Design (QbD) and Process Analytical Technology (PAT)). Empirical regime maps represent the most effective current modelling approach for applying QbD [2] and will be discussed further below. There is a large parametric space of screw designs, formulations, feed arrangements and operating conditions. The additional major technical challenge is that APIs constitute typically 5 - 80% of the ingredients and, consequently, the current empirical approach for developing a satisfactory process for a given formulation is relatively slow and involves considerable costs, particularly for expensive APIs. It may lead to sub-optimal process specifications; for example, decreasing segregation during downstream powder handling by reducing oversized and unwanted fines is proving to be particularly difficult [1]. The mixing by KEs is important for dispersing viscous binders and can be reduced in intensity by incorporating the binder in the powder feed as solid particles and injecting water, rather than as an aqueous solution of the binder, which is considerably more viscous for commonly used polymeric binders [3]. However, more work is required to optimise this approach.

Granule growth and breakdown mechanisms have been identified for HSG [4] and they have been mapped against dimensionless groups incorporating the binder droplet penetration time and granule yield stress respectively. Such regime maps provide a useful tool for designing wet granulation processes by predicting the granule formation mechanism and hence the granule shape and size distribution from a few dimensionless groups based on formulation properties and process parameters. A similar approach has been suggested for TSG [5] but establishing the evolution of the groups along the screws would require discrete particle modelling. The Distinct Element Method (DEM) has been applied to modelling granule growth in HSG via coalescence but was based on empirical rebound criteria involving a measured dynamic yield stress for single DEM particles that represent granules [6]. While it is possible to model wet agglomerate collisions at the primary particle scale using DEM [7], this method has a number of limitations that include the inability to model: (a) the funicular and capillary saturated states, (b) liquid interface merging during, for

example, powder wetting and agglomerate densification, (c) complete drainage of fluid lubricated particles to allow solid-solid contacts to form, (d) viscous forces with interparticle gaps that are greater than that required by the lubrication limit and (e) elastohydrodynamic coupling. Moreover in the case of DEM, (a) the tangential viscous force is approximated by the gap corresponding to the squeeze flow component in the lubrication limit [7] and (b) spherical particles are generally simulated since it is a limitation of the available interaction laws, although more complex shapes can be created by clustering, for example.

The long-term objective of the current work is to develop a Fast Multi-pole Boundary Element Method (FMBEM) code to overcome the above limitations of DEM for application to TSG; a brief description of this method is given in §2. FMBEM is computationally more expensive than DEM and, hence, DEM will be remain the most appropriate method for many large-scale applications. However, DEM requires some features of particle-particle and fluid-particle interactions to be known *a priori* whereas FMBEM can capture them from first principles. For example, FMBEM allows a more realistic estimation of the interparticle gap developed during oblique collisions by allowing the pressure developed in the converging flow at the inlet of the sliding contact to be computed. Given the large number of primary particles in a TSG process, a parallel FMBEM GPU code is being written that will be able to simulate sections of an extruder in a way that is analogous to a recent experimental study [8].

The aim of the current paper is to describe the applicability and advantages of FMBEM to wet granular systems since this method has not been considered previously in the powder technology community. In addition, three different single particle systems will be described in order to exemplify such applications that are also useful as benchmarks: (i) a rigid spherical particle interacting with a thin inviscid liquid film, (ii) an elastic spherical particle fully immersed in a Newtonian liquid moving towards a rigid wall with van der Waals attraction and (iii) a rigid spherical particle sliding tangentially against a rigid wall while immersed in a Newtonian liquid under a constant normal force and at a constant velocity.

2. FMBEM: methodology

The Boundary Element Method (BEM) is a numerical technique for solving linear partial differential equations. Only the boundaries, sources and sinks are meshed, potentially offering significant computational savings compared with the Finite Discrete Element Method (FDEM) [9]. However, BEM typically leads to dense matrices, while for FDEM they are generally sparse and it acts to limit the possible savings for BEM. The Fast Multipole Method (FMM) [10] adopts a hierarchical tree data structure that can reduce the complexity for *N*-body problems when applied to

BEM. Essentially, FMBEM reduces the density of the matrices and enables significant hardware savings compared with BEM [11]. With these savings FMBEM has been demonstrated to be able to solve problems where hundreds of thousands to millions of particles are required with modest resources [12]. The implementation used throughout this work utilizes novel FMBEM software for use on local and massively parallel GPU clusters. To the authors knowledge such commercial codes not available and there are only two FMBEM codes for GPU architectures available worldwide. The implementation used here was developed specifically to address typical wet granular systems. A dynamic optimizer ensures that the FMBEM code runs on a GPU cluster efficiently and with high utilization. More details about the scheme developed are given in the Appendix.

In summary, BEM is extremely efficient since the surfaces, rather than the volumes of the particles are discretised to solve the Green's functions for the fluid velocity field, which avoids the need to mesh the continuous phase or the interior of the particles. This involves a superposition of the fields produced by appropriate point sources and sinks, and dipoles at the corresponding interfaces. FMBEM has greatly enhanced the computational efficiency by allowing the Green's functions to be integrated for the near (particle domain) and far (bulk domain) fields separately (the computational cost scales as $N\log(N)$ rather than N^3 for BEM). It has been applied to some relatively simple systems, such as emulsions [13] and, particularly the dynamics of biological cells and microcapsules [12]. BEM is restricted to Stokes flows (Re < 1: Re = Reynolds number) so that the inertia of the continuous phase (not the particles) is ignored but it could be applied to many systems (e.g. for 10 μm diameter particles, the upper limit of the approach velocity is 10 m/s). Although, BEM was originally developed for linear constitutive equations it has been adapted for nonlinear elastic [14] and viscoelastic [15] material models. It is also possible, for example, to create particles of any shape or to remove liquid from a system resulting from evaporation, desorption or permeation by an array of point sinks on a boundary.

3. Partially submerged rigid spherical particle on a thin film

A rigid spherical particle of radius, R, and density, ρ_S, is allowed to come into contact with an infinite inviscid liquid film of thickness, $T = 2.4R$ with a surface tension, γ, and density, $\rho_B > \rho_A$, corresponding to a half-filling angle $\psi = 0$ at first contact (Fig. 1); the contact angle between the liquid and particle is $\theta_C = 90^{\mathrm{o}}$. Above the liquid film is a second fluid with a density, ρ_A. The interface couples the liquid response as proposed by Landau & Lifshitz [16] and leads to a change in the minimum gap, D, between the particle and wall. The version of the interface coupling utilized by Ladau & Lifshitz [16] includes a viscous interaction term that is incorporated in the FMBEM implementation but neglected in the numerical solver of the Laplace-Young equation. When an

equilibrium gap is achieved, the particle is displaced towards the wall at a velocity 0.1 μm/s until contact is made with the wall. It is then allowed to return to the equilibrium gap under the action of buoyancy.

The FMBEM algorithm returns the force on the particle and corresponding minimum gap at each time step. The dimensionless capillary force, $F_C^* = F^C/R\gamma$, where F_C is the capillary force, is calculated from the Laplace-Young equation as:

$$F_C^* = 2\pi \sin(\pi - \psi - \theta_C)\sin(\psi) \quad (1)$$

The capillary length is given by $\lambda_C = \sqrt{(\rho_B - \rho_A)g/\gamma}$, where g is the acceleration due to gravity, and hence the system is uniquely described by four parameters: (i) the Bond number $B = (R/\lambda_C)^2 = 11.04$, density difference $\rho = (\rho_S - \rho_A)/(\rho_B - \rho_A) = 2$, contact angle $\theta_C = 90^o$ and dimensionless film thickness $T^* = T/\lambda_C = 7.37$.

The dimensionless capillary force as a function of the dimensionless gap is shown in Fig. 2.The results are in excellent agreement with Eq. (1); the relative error is of the order of the numerical error $O(10^{-6})$. For this special case with $\theta_C = 90^o$, the result is symmetric about $D/R = 1.21$. The particle first touches the surface of the liquid at $D/R = 2.21$ and the liquid then wets the particle so that it is displaced away from the wall due to buoyancy with an unstable equilibrium position of $D/R = 2.43$; the solution of Laplace-Young equation has both a stable and unstable branch [17]. Since the acceleration is zero, perturbation forces do not cause a transition to the stable branch that would probably occur in a real experiment. When it is moved towards the wall, the capillary force exhibits a maximum value before touching the wall. The particle is then allowed to move away from the wall under the action of buoyance when a stable equilibrium is achieved with a half-filling angle of 162^o and a gap of $D/R = 0.21$.

4. Elastic spherical particle fully immersed in a fluid moving towards a rigid wall with van der Waals attraction

The time taken for a spherical particle to reach a wall under low Reynold's number conditions is known to be infinite [18]. However, it is finite when there is an attractive force such as a van der Waals potential. A schematic of the problem is shown in Fig. 3. This example demonstrates the complete drainage of a fluid between two solid surfaces. Any multi-particle solver should require techniques for resolving collisions in which there is exclusion of liquid between particles and this example is one of the simplest demonstrations. Here, the time taken for a 1 μm radius spherical

particle, with density 2200 kg/m^3, to contact a wall when immersed in Newtonian liquid with an initial velocity 2.8 mm/s and minimum gap 4.2 μm is obtained by three different methods: Chan and Horn's inertia-less calculation [18], a numerical solver for the Newtonian equations including the inertia of the particle and the FMBEM code that also includes the inertia of the particle. For all three methods, the van der Waals attractive force is represented by the following expression [19]:

$$F_{vdW} = -\frac{RA}{6D^2} \tag{2}$$

where A = 3 x 10^{-19} J is the Hamaker constant.

Chan and Horn's [18] inertia-less calculation has the following form:

$$D(t) = \left[\frac{A}{18\pi\eta R}(t_c - t)\right]^{1/2} \tag{3}$$

where $\eta = 1$ Pa.s is the fluid viscosity and t_c is the finite contact time and t is the time. The results of the numerical inertia solution were obtained by solving the following force balance using Matlab's ODE 45 numerical solver:

$$\frac{6\pi\eta R}{D(t)}\frac{dD}{dt} + \frac{RA}{6D^2(t)} = m\frac{d^2D(t)}{d(t^2)} \tag{4}$$

where m is the particle mass.

Chan and Horn's inertia-less calculation is an upper bound on the time for the particle to reach the wall since inertia acts to continue the motion towards the wall more rapidly than would otherwise be the case as can be seen in Fig. 4. The travel duration from the numerical solution of Eq. (3) is slightly greater than a factor 0.58 less than that predicted by the theory of Chan and Horn [18]. The figure also shows that there is a close agreement with the FMBEM calculation of the trajectory with the numerical solution of Eq. (4). That the particle is able to contact the wall even though the viscous force, F_V , scales as $1/D$ (Eq. (5) [18] arises because the van der Waals force scales as $1/D^2$ (Eq. (2)) so that at small gaps the attractive force dominates.

$$F_V = -\frac{6\pi\eta R^2}{D}\frac{dD}{dt} \tag{5}$$

5. Hydrodynamic lubrication

Provided that the normal force is sufficiently small, and the liquid viscosity, sliding velocity and radii are sufficiently large, hydrodynamic lubrication will be developed between two particles undergoing an oblique impact. This is termed *isoviscous hydrodynamic lubrication* (IHL) since the typical contact pressures will be insufficient to increase the viscosity of the liquid unlike those that are prevalent in engineering contacts. However, is possible that the particles are deformed elastically and that has the effect of reducing the contact pressure and hence the viscous resistance to sliding; this is termed *isoviscous elastohydrodynamic lubrication* (IEHL). In the current section, such lubrication is modelled using FMBEM by considering a spherical particle in close proximity to a wall that is immersed in a Newtonian fluid as shown schematically in Fig. 5. A constant velocity parallel to the wall is applied to the particle and the coefficient of friction is evaluated. The mass of the particle is taken to be the normal load on the particle, which is increased by increasing the density of the particle. The FMBEM code is used to calculate the force required to maintain the velocity and the coefficient of friction is determined as follows [20]:

$$\mu = \frac{\oiint \tau_w \, dxdy}{\oiint p dxdy} \tag{6}$$

where μ is the coefficient of friction (due to lubrication), τ_w is the wall shear stress acting on the surface of the particle and p is the pressure on the walls.

Figures 6 and 7 show the calculated coefficients of friction as a function of the non-dimensional group $(\eta v R/W)$, where W is equal to the weight of the particle and v is the imposed sliding velocity, for particles having Young's moduli of 10 GPa and 1 MPa respectively. Adams & Edmondson [21] derived a closed-form approximation for a rigid particle (HL) that may be written as follows:

$$\mu = \frac{\pi \eta v R}{W} \left\{ 1.22 \sinh^{-1} \left(0.04 \frac{\pi \eta v R}{W} + 0.59 \right) \right\} \tag{7}$$

It may be seen in Fig. 6 that Eq. (7) is a reasonable approximation to that calculated by the FMBEM. However, at small values of the dimensionless group, this equation overestimates the coefficient of friction because the onset of elastic deformation of the particle induces IEHD lubrication. de Vincente et al. [22] obtained the following closed-form approximation for the IEHD limit that may be written as:

$$\mu = 2\left\{3.2\left(\frac{3\eta v}{8ER}\right)^{0.71}\left(\frac{3W}{8ER^2}\right)^{-0.76} + 0.96\left(\frac{3\eta v}{8ER}\right)^{0.36}\left(\frac{3W}{8ER^2}\right)^{-0.11}\right\} \quad (8)$$

It may be seen in Fig. 7 that the agreement between Eq. (8) and the FMBEM calculation is excellent. The corresponding pressure profile is shown in Fig. 8. At the rear of the contact the pressure is negative, which corresponds to the Sommerfield solution for a 2D journal bearing [23]. In practise, the negative pressure will result in cavitation.

Thus it has been demonstrated that FMBEM is capable of calculating the friction between hydrodynamically lubricated particles; Figs 6 and 7 represent a region of a form of a Stribeck curve [23]. In a complete version of such a curve, small values of the group $(\eta v R/W)$ are associated with boundary friction while, and with increasing values of the group, eventually there will be a transition to the hydrodynamic region; this transition region is term *mixed lubrication*. Since it has been shown that FMBEM is able to model the complete drainage between particles immersed in a liquid, it would be straightforward to model the complete Stribeck curve. This is relevant since it has been established that wet particle assemblies exhibit a transition from frictional to lubricated flow, for example, with increasing strain rate. Thus Iveson *et al.* [24] studied the axial compression of cylindrical agglomerates of densely packed fine glass ballotini (~ 35 μm) with water, glycerol and a series of silicone oils as liquid binders to provide a range of viscosities and surface tensions. It was observed that at small values of the Capillary number ($\mathrm{Ca} = \eta\dot{\epsilon}R/\dot{\gamma}\cos\theta_C$ where $\dot{\epsilon}$ is the nominal uniaxial strain rate) the strength of the agglomerates was constant but at some critical value it increased with increasing Ca. The initial region was interpreted as corresponding to interparticle friction and the second region as being dominated by viscous forces. That is, there is a clear indication of a transition from frictional to lubricated flow as expected from the trends in a Stribeck curve. Huang *et al.* [25] measured the shear behaviour of monodisperse polystyrene beads (~290 μm) with an isodense liquid binder having viscosities in the range 1 - 2300 mPa s. They also observed a frictional to lubricated transition at a critical shear rate that decreased linearly with increasing binder viscosity.

It may be concluded from the above studies that discrete modelling of the deformation characteristics of wet agglomerates, which are critical to the performance of TSG, should account for transitions from the frictional to the lubricated state and vice-versa. This is a particular advantage of FMBEM compared with DEM, which relies on the equation derived by Goldman et al. [26, 27] to calculate the hydrodynamic tangential force between particles. It is based on an asymptotic solution of the Stokes equation and is only applicable in the lubrication limit. As mention in §1, it requires knowledge of the interparticle gap, which is obtained from that calculated by the normal interaction using a solution

based on the lubrication approximation. Thus unlike DEM, the calculation is not fully coupled in addition to neglecting the role of IEHL, which may also be important in normal collisions [28]. Real particles are topographically rough so it is important to emphasise that the transition from frictional to lubricated sliding is governed by the dimensionless film thickness parameter being ~ 5; it is defined by the ratio of the minimum film thickness to a combined asperity height parameter as represented by a minimum gap that acts as a cut-off distance [29].

6. Conclusions

The validation of the current FMBEM code has been demonstrated using examples that are relevant to wet granular dynamics. Although the problems presented here are simplistic, they demonstrate that FMBEM is able to compute wet particle interactions that occur frequently in multi-particle granular dynamics. In particular, it is possible to account for frictional-hydrodynamic transitions that are important for the behaviour of wet agglomerates and, consequently, for the performance of TSG processes. In summary, it has been shown that FMBEM is able to accurately (a) model low Reynolds number fluid flow efficiently, (b) track and evolve liquid and elastic interfaces, (c) account for drainage between hydrodynamically lubricated particles and (d) effectively solve elastohydrodynamic problems. Thus, FMBEM has many advantages compared with DEM but at a significant computational cost.

Acknowledgements

The authors are grateful for the funding provided by EPSRC (EP/M02959X: Discrete computational modelling of twin screw granulation).

References

[1] A. S. El Hagrasy, J. R. Hennenkamp, M. D. Burke, J. J. Cartwright, J. D. Litster, Twin screw wet granulation: influence of formulation parameters on granule properties and growth behaviour, Powder Technol. 238 (2013) 108-115.

[2] D. Kayrak-Talay, S. Dale, C. Wassgren, J.D. Litster, Quality by design for wet granulation in pharmaceutical processing: assessing models for a priori design and scaling, Powder Technol. 240 (2013) 7-18.
[3] R.M. Dhenge, K. Washino, J. Cartwright, M.J. Hounslow, A.D. Salman, Twin screw granulation using conveying screws: Effects of viscosity of granulation liquids and flow of powders, Powder Technol. 238 (2013) 77-90.
[4] S.M. Iveson, A.L. Philippe, S.F. Wauters, J.D. Litster, G.M.H. Meesters, B. Scarlett. Growth regime map for liquid-bound granules: further development and experimental validation, Powder Technol. 117 (2001) 83-97.
[5] R.M. Dhenge, K. Washino, J. Cartwright, M.J. Hounslow, A.D. Salman, Twin screw granulation using conveying screws: Effects of viscosity of granulation liquids and flow of powders, Powder Technol. 238 (2013) 77.
[6] Gantt JA, Cameron IT, Litster JD, Gatzke EP. Determination of coalescence kernels for high-shear granulation using DEM simulations. Powder Technol. 170 (2006) 53.
[7] G. Lian, C. Thornton, M.J. Adams, Discrete particle simulation of agglomerate impact coalescence, Chem. Eng. Sci. 53 (1998) 3381-3391.
[8] M. Verstraeten, D.V. Hauwermeiren, K. Lee, N. Turnbull, D. Wilsdon, M.am Ende, P. Doshi et al., In-depth experimental analysis of pharmaceutical twin-screw wet granulation in view of detailed process understanding, Int. J. Pharm. 15 Jul. (2017).
[9] A.A. Munjiza, The Combined Finite-Discrete Element Method, John Wiley & Sons, Chichester, UK, 2005.
[10] L. Greengard, V. Rokhlin, A fast algorithm for particle simulations, J. Comput. Phys. 73 (1987) 325-348.
[11] Y.J. Liu, N. Nishimura, The fast multipole boundary element method for potential problems: a tutorial, Eng. Anal. Bound. Elem. 30 (2006) 371-381.
[12] Pozrikidis C. Computational hydrodynamics of capsules and biological cells. CRC Press, 1st edition, 2010.
[13] A.Z. Zinchenko, R.H. Davis, Shear flow of highly concentrated emulsions of deformable drops by numerical simulations, J. Fluid Mech., 455 (2002) 21-61.
[14] G. Beer, I. Smith, C. Duenser, The Boundary Element Method with Programming: for Engineers and Scientists, Springer, Germany, 2008.
[15] T. T-L Thye-Lai, J. Connor, D.A. Antoniadis, A viscoelastic bem for modeling oxidation. COMPEL: Int. J. Comp. Math. Elect. Electronic Engng., 6 (1987) 115-121.

[16] Landau LD, Lifshitz, EM. Course of Theoretical Physics, vol. 6, second edition, Pregamon Press, Oxford, 2013.
[17] G. Lian, C. Thornton, M.J.Adams, A theoretical study of liquid bridge forces between two rigid spherical bodies. J. Coll. Int. Sci., 161 (1993) 138-147.
[18] D.Y.C. Chan, R.G. Horn. The drainage of thin liquid films between solid surfaces, J. Chem. Phys., 83 (1985) 5311-5324.
[19] J.N. Israelachvili,Intermolecular and Surface Forces. Academic Press; 2015.
[20] B, Jacod, Friction in elasto-hydrodynamic lubrication, Publisher: FEBOdruk B. V., Enschede (1976).
[21] M.J. Adams, B. Edmondson, B. Forces between particles in continuous and discrete liquid media in Tribology in Particulate Technology. B.J. Briscoe, M.J. Adams, (eds) Adam Hilger, Bristol (1987) pp 154-172.
[22] J. De Vicente, J.R. Stokes, H.A. Spikes, The frictional properties of Newtonian fluids in rolling–sliding soft-EHL contact. Trib. Lett. 20 (2005) 273-286.
[23] I.M. Hutchings, P. Shipway, Tribology: friction and wear of engineering materials. Second Edition, Butterworth-Heinemann, (2017).
[24] S.M. Iveson, J.A. Beathe, N.W. Page The dynamic strength of partially saturated powder compacts: the effect of liquid properties, Powder Techno. 127 (2002): 149-161.
[25] N. Huang, G. Ovarlez, F. Bertrand, S. Rodts, P. Coussot, D. Bonn. Flow of wet granular materials, Phys. Rev. Lett. 94 (2005) 028301.
[26] A.J. Goldman, R.G. Cox, H.Brenner, Slow viscous motion of a sphere parallel to a plane wall—I Motion through a quiescent fluid. Chem. Eng. Sci., 22 (1967) 637-651.
[27] A.J. Goldman, R.G. Cox, H.Brenner, Slow viscous motion of a sphere parallel to a plane wall—II Motion through a quiescent fluid. Chem. Eng. Sci., 22 (1967), 653-660.
[28] G. Lian, M. J. Adams, C. Thornton, Elastohydrodynamic collisions of solid spheres, J. Fluid Mech. 311 (1996): 141-152.
[29] B.J. Hamrock, Fundamentals of fluid film lubrication. McGraw-Hill, New York (1994)

Appendix

Summary of the formulation of the FMBEM code.

The numerical scheme is a more advanced version of that described in FMBEM to determine the matrices on which the solver acts. The solver was a GPU version of GMRes with incomplete LU-factorization [29]. Adaptive h-p mesh refinement was employed [30]. The time step for each simulation was the minimum of a number of a semi-analytic expressions to identify the smallest time step size for continued simulation. Generally this corresponded to the smallest of the distance-travelled/(1000*velocity) being used for the time step. However the distance travelled could be the distance for collision or the movement of an interface near a solid contact.

[29] Youcef Saad and Martin H. Schultz, GMRES: A Generalized Minimal Residual Algorithm for Solving Nonsymmetric Linear Systems, SIAM Journal on Scientific and Statistical Computing, 1986, Vol. 7, No. 3 : pp. 856-869

[30] Rank E. Adaptive h-, p-and hp-versions for boundary integral element methods. International Journal for Numerical Methods in Engineering 1989; 28(6):1335–1349.

Figures:

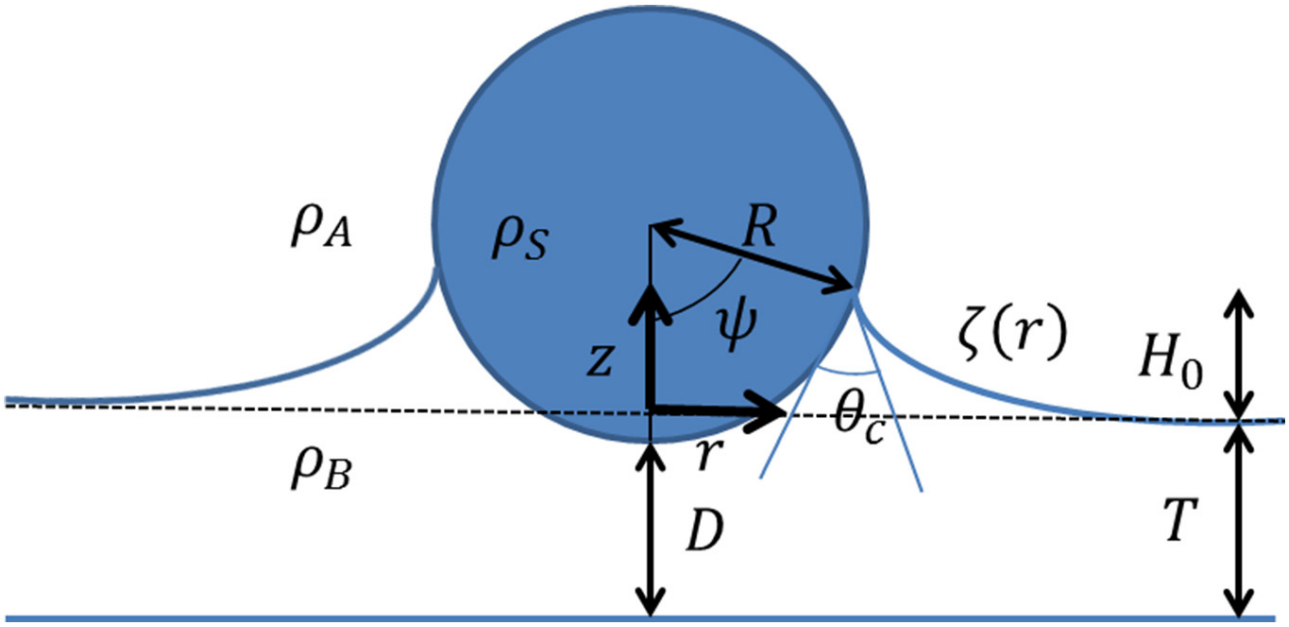

Fig. 1. Schematic of geometry and parameters for the determination for a partially immersed rigid spherical particle where $\zeta(r)$ is the liquid free-surface profile, H_0 is the capillary rise/fall, r is the radial coordinate and z is the vertical coordinate. The position of the interface is given by $(r, \zeta(r))$.

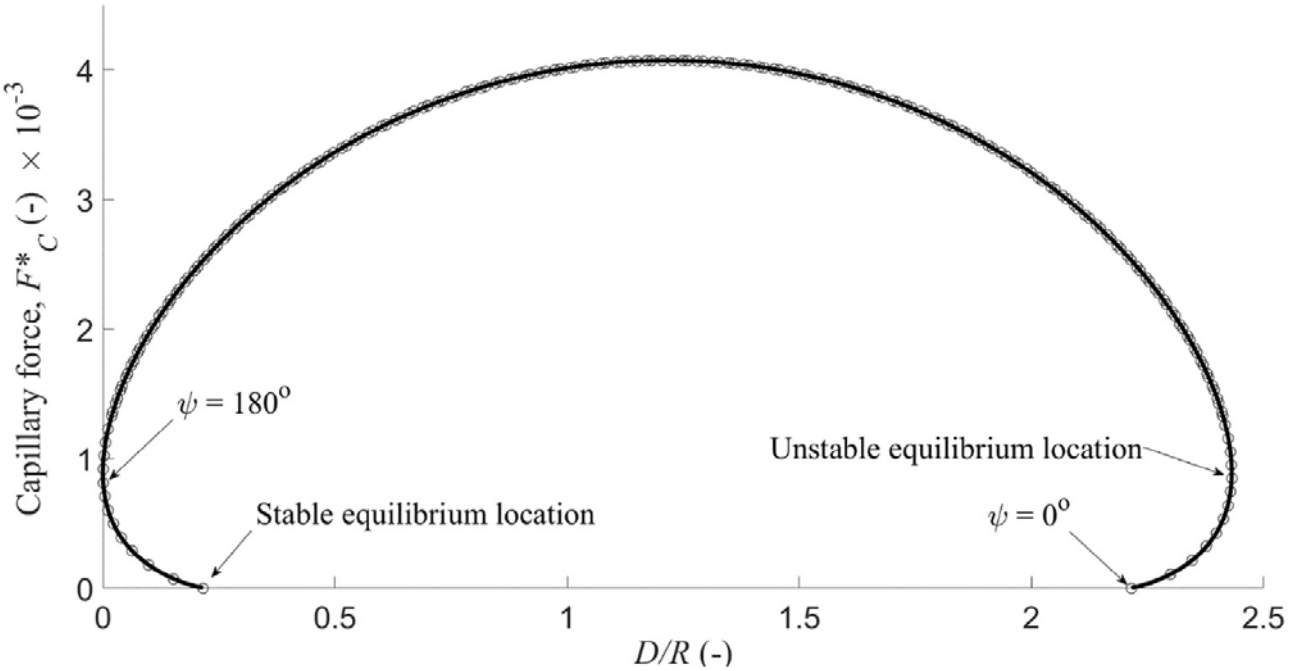

Fig. 2. The non-dimensional capillary force as a function of the dimensionless gap calculated by and the numerical solution (line) and the FMBEM code (circles).

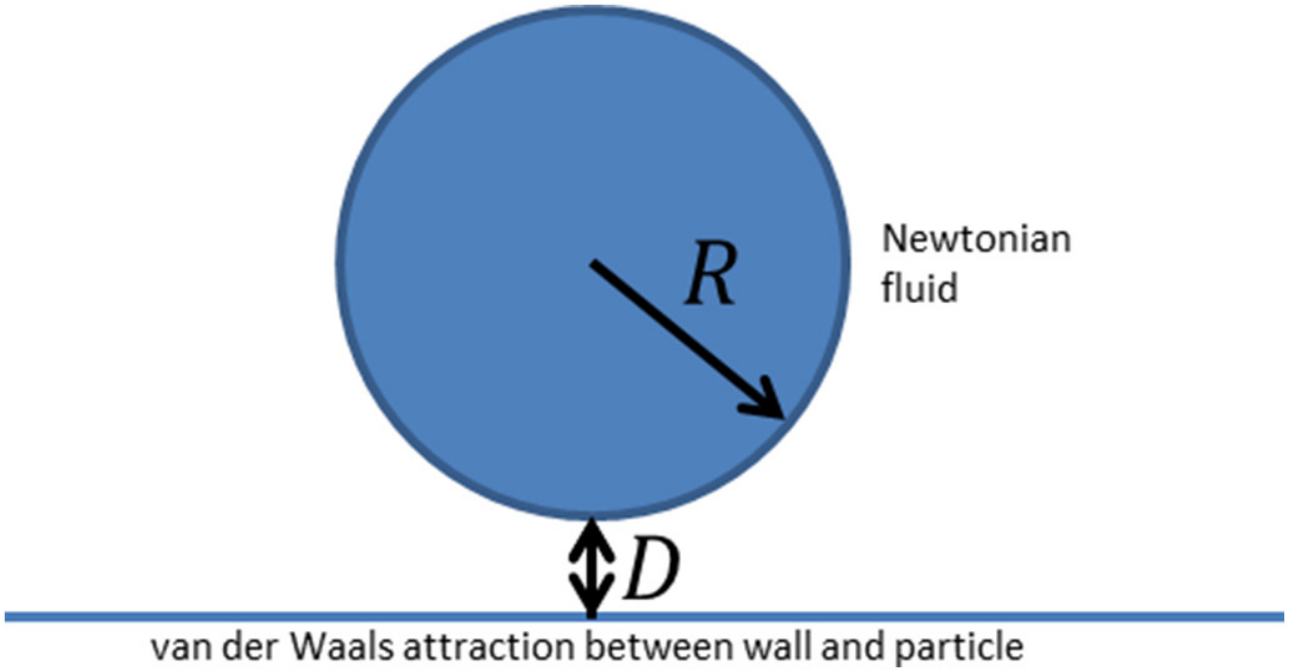

Fig. 3. Schematic diagram of van der Waals attraction between a spherical particle and a wall immersed in a Newtonian liquid.

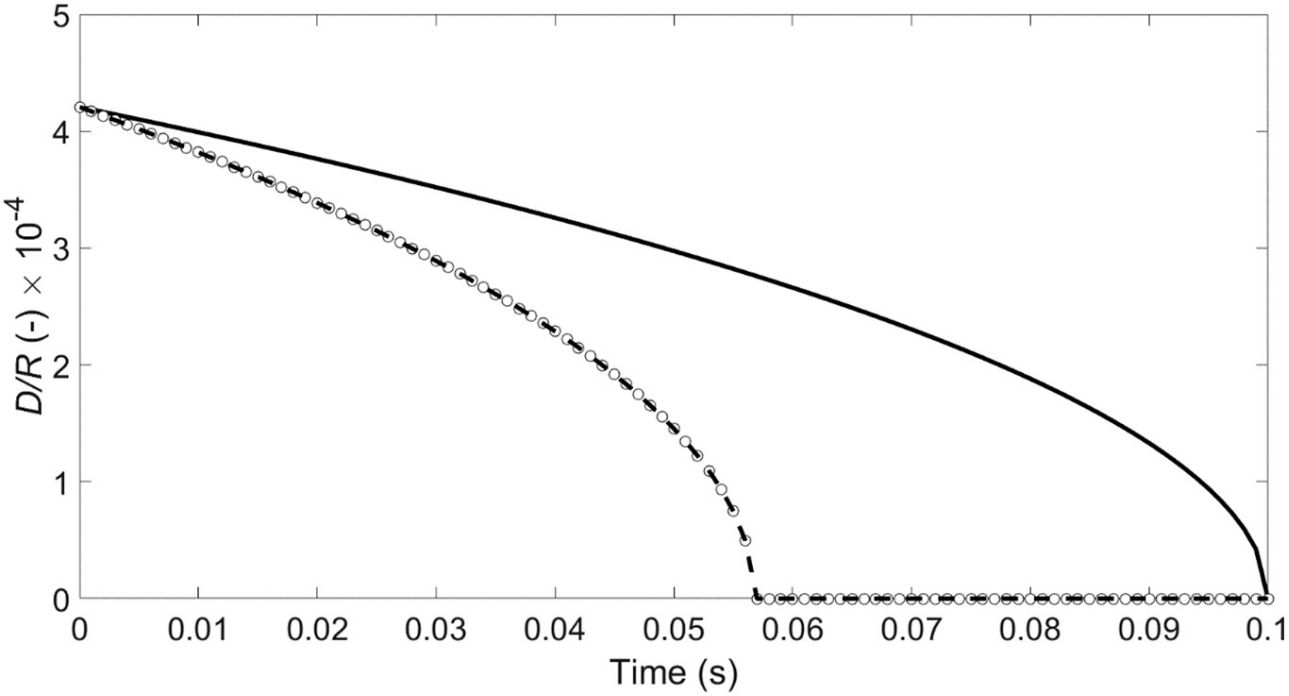

Fig. 4. Dimensionless minimum gap between a spherical particle and wall calculated for the system shown in Fig. 3 where the full line refers to Chan and Horn [18] solution (Eq. 4), the full circles correspond to the numerical solution of Eq. (4) and the dashed line was calculated using FMBEM.

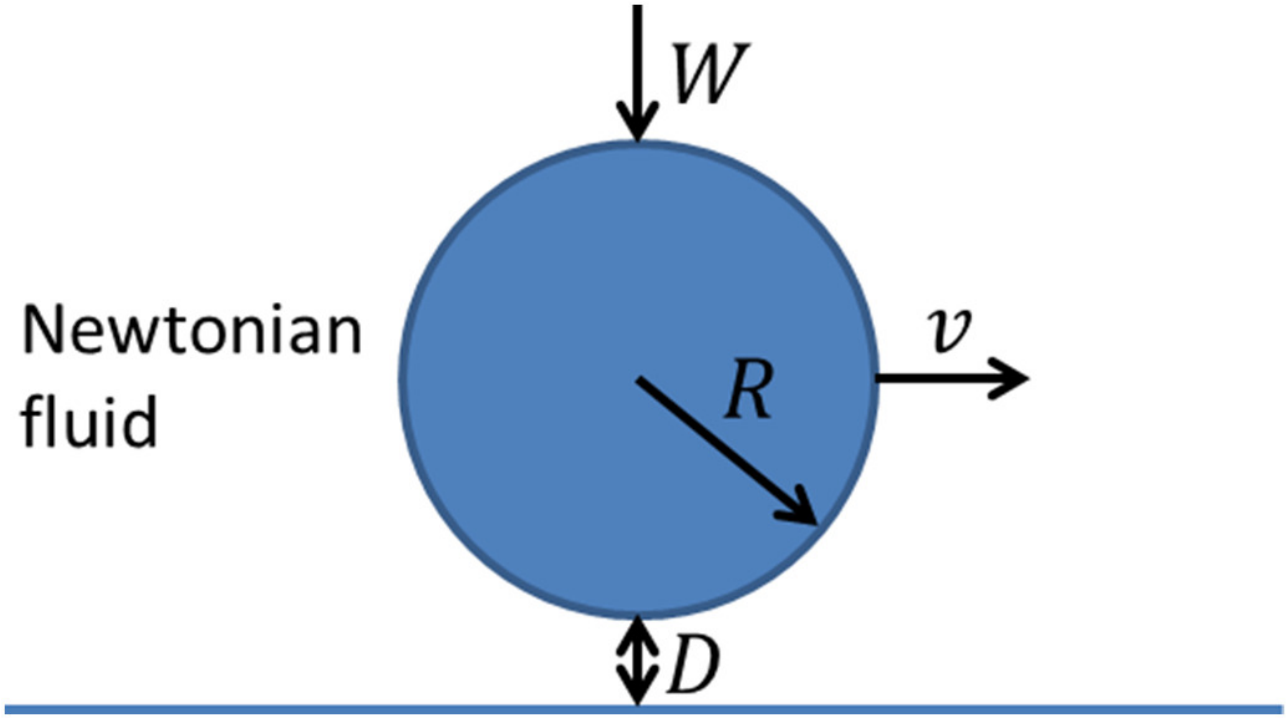

Fig. 5. Schematic diagram of a hydrodynamically lubricated spherical particle where W is the normal force and v is the sliding velocity.

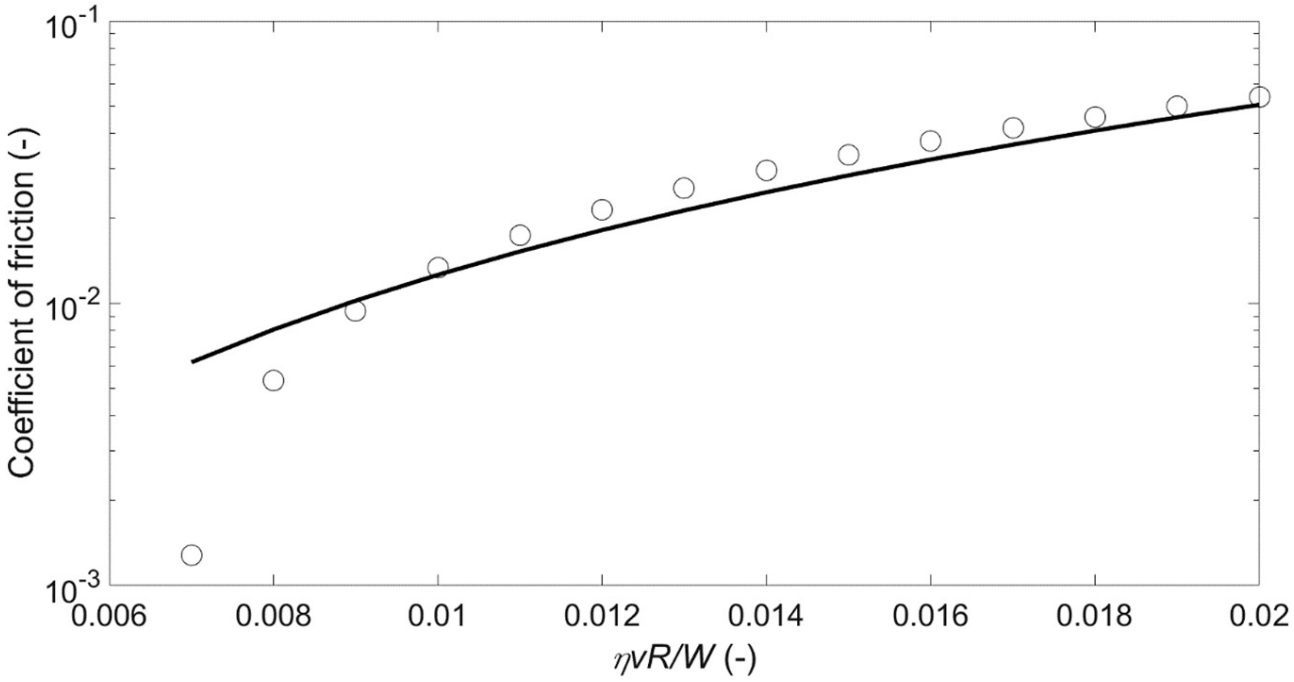

Fig. 6. The coefficient of friction as a function of the non-dimensional group ($\eta vR/W$) calculated by FMBEM (full circles) and by Eq. (7) for IHL (full line); the Young's modulus of the particle is 10 GPa.

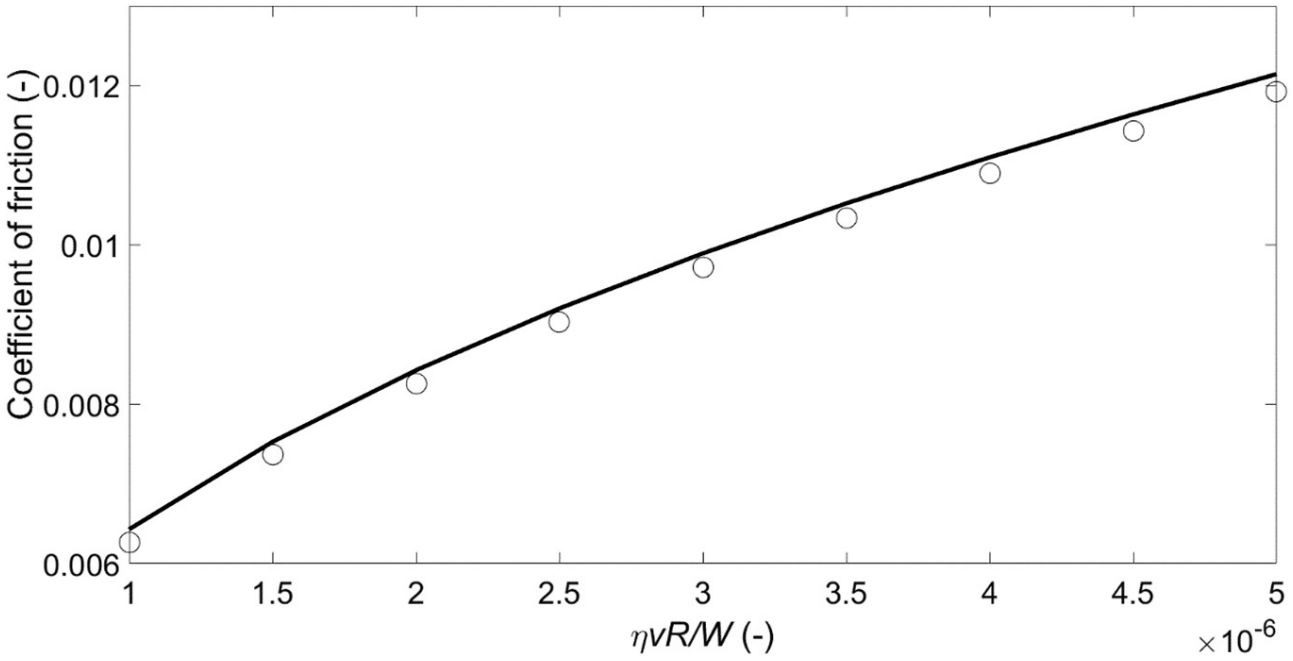

Fig. 7. The friction coefficient as a function of the the non-dimensional group ($\eta vR/W$) calculated by FMBEM (full circles) and by Eq. (8) for IEHD (full line); the Young's modulus of the particle is 1 MPa.

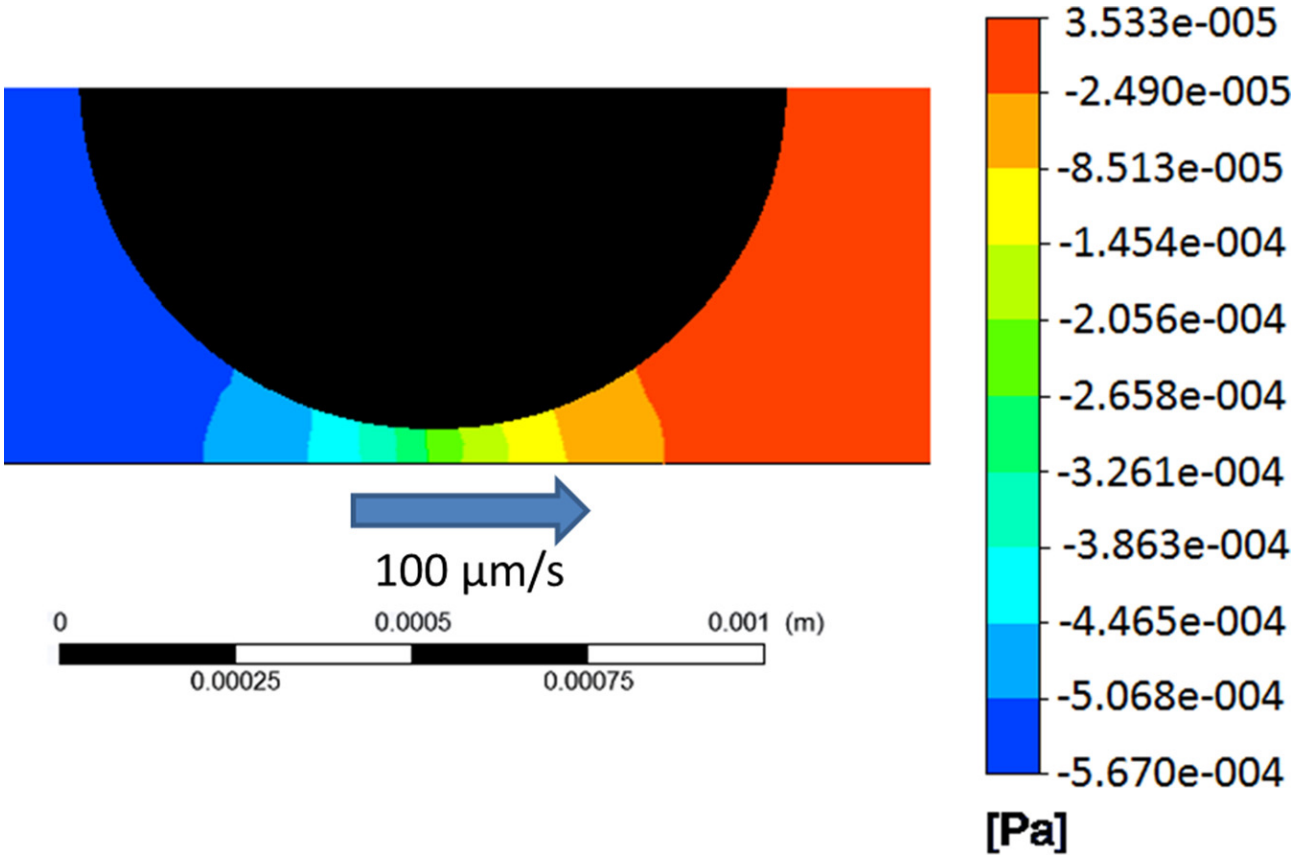

Fig. 8. Fluid pressure profile for a sliding spherical particle in a Newtonian liquid.